Phytoplankton dynamics in contrasting early stage North Atlantic spring blooms: composition, succession, and potential drivers

C. J. Daniels,[1,*] A. J. Poulton,[2] M. Esposito,[2] M. L. Paulsen,[3] R. Bellerby[4,5,6], M. St John[7] and A. P. Martin[2]

[1] {Ocean and Earth Sciences, National Oceanography Centre Southampton, University of Southampton, UK}

[2] {Ocean Biogeochemistry and Ecosystems, National Oceanography Centre, University of Southampton Waterfront Campus, UK}

[3] {Department of Biology, Marine Microbiology Department, University of Bergen, Norway}

[4] {Norwegian Institute for Water Research (NIVA), Bergen, Norway}

[5] {Uni Bjerknes Centre, Bergen, Norway}

[6] {State Key Laboratory for Estuarine and Coastal Research, East China Normal University, China}

[7] {National Institute of Aquatic Resources, Technical University of Denmark, Charlottenlund, Denmark}

* Correspondence to: C. J. Daniels (c.daniels@noc.soton.ac.uk)

Running head: Spring Bloom Phytoplankton Composition

Abstract

The spring bloom is a key annual event in the phenology of pelagic ecosystems, making a major contribution to the oceanic biological carbon pump through the production and export of organic carbon. However, there is little consensus as to the main drivers of spring bloom formation, exacerbated by a lack of in situ observations of the phytoplankton community composition and its evolution during this critical period.

We investigated the dynamics of the phytoplankton community structure at two contrasting sites in the Iceland and Norwegian Basins during the early stage (25th March - 25th April) of the 2012 North Atlantic spring bloom. The plankton composition and characteristics of the initial stages of the bloom were markedly different between the two basins. The Iceland Basin (ICB) appeared well mixed to > 400 m, yet surface chlorophyll *a* (0.27-2.2 mg m^{-3}) and primary production (0.06-0.66 mmol C m^{-3} d^{-1}) were elevated in the upper 100 m. Although the Norwegian Basin (NWB) had a persistently shallower mixed layer (< 100 m), chlorophyll *a* (0.58-0.93 mg m^{-3}) and primary production (0.08-0.15 mmol C m^{-3} d^{-1}) remained lower than in the ICB, with picoplankton (< 2 µm) dominating chlorophyll *a* biomass. The ICB phytoplankton composition appeared primarily driven by the physicochemical environment, with periodic events of increased mixing restricting further increases in biomass. In contrast, the NWB phytoplankton community was potentially limited by physicochemical and/or biological factors such as grazing.

Diatoms dominated the ICB, with the genus *Chaetoceros* (1-166 cells mL^{-1}) being succeeded by *Pseudo-nitzschia* (0.2-210 cells mL^{-1}). However, large diatoms (> 10 µm) were virtually absent (< 0.5 cells mL^{-1}) from the NWB, with only small nano-sized (< 5 µm) diatoms (i.e. *Minidiscus* spp.) present (101-600 cells mL^{-1}). We suggest micro-zooplankton grazing, potentially coupled with the lack of a seed population of bloom forming diatoms, was restricting diatom growth in the NWB, and that large diatoms may be absent in NWB spring blooms. Despite both phytoplankton communities being in the early stages of bloom formation, different physicochemical and biological factors controlled bloom formation at the two sites. If these differences in phytoplankton composition persist, the subsequent spring blooms are likely to be significantly different in terms of biogeochemistry and trophic interactions throughout the growth season, with important implications for carbon cycling and organic matter export.

1. Introduction

The spring bloom is a key annual event in the phenology of pelagic ecosystems, where a rapid increase in phytoplankton biomass has a significant influence on upper ocean biogeochemistry and food-availability for higher trophic levels (Townsend et al., 1994; Behrenfeld and Boss, 2014). Spring blooms are particularly prevalent in coastal and high latitude waters. The high levels of phytoplankton biomass and primary production that occur during these blooms, and its subsequent export out of the surface ocean, result in a significant contribution to the biological carbon pump (Townsend et al., 1994; Sanders et al., 2014). The North Atlantic spring bloom is one of the largest blooms on Earth, making a major contribution to the annual export of ~1.3 Gt C yr^{-1} from the North Atlantic (Sanders et al., 2014). The timing and magnitude of the spring bloom can have a significant biogeochemical impact (Henson et al., 2009); hence it is important to understand both the controls on, and the variability in, bloom timing, magnitude and community structure. Despite its importance, there remains little consensus as to the environmental and ecological conditions required to initiate high latitude spring blooms (Townsend et al., 1994; Behrenfeld, 2010; Taylor and Ferrari, 2011b; Smyth et al., 2014).

Phytoplankton blooms occur when growth rates exceeds loss rates (i.e. a sustained period of net growth); phytoplankton growth rate constraints include irradiance, nutrient supply, and temperature, while losses can occur through predation, advection, mixing out of the euphotic zone, sinking and viral attack (Miller, 2003). Therefore, the rapid increase in (net) growth rates during the spring bloom must be due to either an alleviation of those factors constraining growth, a reduction in factors determining losses, or (more likely) some combination of both.

The critical depth hypothesis (Sverdrup, 1953), the seminal theory of spring bloom initiation, proposes that there exists a critical depth such that when stratification shoals above this depth, phytoplankton growth will exceed mortality and a bloom will occur. However, this hypothesis has been more recently brought into question as bloom formation has been observed to start earlier than expected (Mahadevan et al., 2012), and in the absence of stratification (Townsend et al., 1992; Eilertsen, 1993). Several new theories have now been developed to explain these occurrences (reviewed in Behrenfeld and Boss, 2014; Fischer et al., 2014; Lindemann and St. John, 2014).

Eddies and oceanic fronts have both been identified as sources of stratification prior to the wider onset of seasonal stratification (Taylor and Ferrari, 2011a; Mahadevan et al., 2012). However, they do not explain blooms in the complete absence of stratification, which can instead be explained by the critical turbulence hypothesis (Huisman et al., 1999; Taylor and Ferrari, 2011b; Brody and Lozier, 2014; Smyth et al., 2014). These theories distinguish between a convectively driven actively mixed layer and a density-defined mixed layer such that if convective mixing reduces sufficiently, blooms can occur in the actively mixing layer although the density-defined mixing layer remains deep. Therefore, blooms are able to form in the apparent absence of stratification, as defined by the presence of a thermocline. An alternative to the hypotheses concerning physical controls on bloom formation is the disturbance-recovery hypothesis proposed by Behrenfeld (2010), which suggests that the decoupling of phytoplankton and microzooplankton contact rates in deep winter mixed layers results in phytoplankton net growth from winter onwards due to reduced mortality (via grazing). It is also possible that there are multiple biological and physical controls, acting on different spatial and temporal scales, that drive the heterogeneous bloom distributions observed via remote sensing (e.g. Lindemann and St. John, 2014).

Significant interannual and decadal variability in the structure and timing of spring blooms in the North Atlantic has been documented (Henson et al., 2009). Such variability in bloom timing has been attributed to the variation in the winter mixed layer depth (WMLD); a deeper WMLD results in a delayed bloom in the subarctic North Atlantic (Henson et al., 2009). A strong latitudinal trend exists in the North Atlantic where the spring bloom propagates north due to seasonal relief from light limitation at high latitudes (Siegel et al., 2002; Henson et al., 2009). Both the role of the WMLD in interannual variability in bloom timing and the northwards progression of bloom start dates highlight how physical processes have a clear and significant impact on bloom formation. The controls on the variability in bloom magnitude are less certain, although it appears to be a combination of WMLD variability influencing the start date as well as biological factors such as phytoplankton composition and grazing (Henson et al., 2009).

Despite considerable discussion on the various factors that may or may not influence bloom initiation, timing, magnitude and phenology, few studies have actually examined the in situ phytoplankton community. Instead, because of the need for temporally resolved data, satellite-derived products and models have been used in much of the previous work on spring

blooms. However, such methods cannot address the potential influence of the complex plankton community structure on the development of a spring bloom.

The traditional text book view of a phytoplankton spring bloom is that the pre-bloom pico-phytoplankton (cells < 2 µm) dominated community is directly succeeded by a diatom dominated community (Margalef, 1978; Barber and Hiscock, 2006); as conditions become more favourable for growth, a diatom bloom develops, 'suppressing' growth of other phytoplankton groups. Through either increased predation, nutrient stress or a changing physical environment (Margalef, 1978), diatoms decline and are then replaced by other phytoplankton such as dinoflagellates and coccolithophores (Lochte et al., 1993; Leblanc et al., 2009). In this way, a series of phytoplankton functional type successions occur as the spring bloom develops. That diatoms often dominate intense spring blooms is well accepted (Lochte et al., 1993; Rees et al., 1999), however the dynamics of the interplay between diatoms and the rest of the community have been questioned (Barber and Hiscock, 2006). The rapid proliferation of diatoms in a spring bloom does not necessarily suppress other phytoplankton (Lochte et al., 1993; Barber and Hiscock, 2006), and the "rising tide" hypothesis states that instead of succession, the favourable conditions for diatoms also favour other phytoplankton groups and therefore all phytoplankton will respond positively and grow (Barber and Hiscock, 2006). The apparent suppression of the phytoplankton community by diatoms is due to the relatively high intrinsic growth rates of diatoms resulting in concentrations dwarfing the rest of the community. The "rising tide" hypothesis is a contrasting theory to succession, however it may be that the phytoplankton community response will not be universal, with some taxa-specific succession due to competition or increased grazing (Brown et al., 2008). Furthermore, succession may appear to occur if phytoplankton loss rates are taxonomically specific, such that while many phytoplankton groups concurrently grow, successive loss of specific groups occurs.

The overall goal of our study was to determine the phytoplankton community structure, and its evolution during the spring bloom in the North Atlantic, linking the community structure to the physical environment and examining whether succession to a diatom dominated environment would occur early in the growth season (March-April). Sampling for this study was carried out as part of the multidisciplinary EuroBASIN "Deep Convection Cruise". The timing and location of this cruise (19th March - 2nd May 2012) was chosen to try and observe the transition from deep winter convection to spring stratification, and examine the physical controls on the dynamics of phytoplankton, carbon export and trophic interactions. A recent

149 study has previously suggested that winter convection in the North Atlantic and Norwegian
150 Sea sustains an overwintering phytoplankton population, thus providing an inoculum for the
151 spring bloom (Backhaus et al., 2003), although this transition has not been explicitly
152 examined before.

153 ## 2. Methods

154 ### 2.1 Sampling

155 The Deep Convection cruise repeatedly sampled two pelagic locations in the North Atlantic
156 (Fig. 1), sited in the Iceland (ICB, 61.50 °N, 11.00 °W) and Norwegian (NWB, 62.83 °N,
157 2.50 °W) Basins, onboard the R/V *Meteor*. The ICB was visited four times, and the NWB
158 visited three times during the course of the cruise. Samples were collected from multiple
159 casts of a conductivity-temperature-depth (CTD) - Niskin rosette, equipped with a
160 fluorometer, at each station. Water samples for rates of primary production (PP), community
161 structure and ancillary parameters (chlorophyll *a* [Chl *a*], calcite [PIC], particulate silicate
162 [$bSiO_2$] and macronutrient concentrations) were collected from predawn (02:30-05:00 GMT)
163 casts from six light depths (55 %, 20 %, 14 %, 7 %, 5 % and 1 % of incidental PAR). The
164 depth of 1 % incident irradiance was assumed to equate to the depth of the euphotic zone
165 (e.g. Poulton et al., 2010). Optical depths were determined from a daytime CTD cast on
166 preceding days at each site. Additional samples for coccolithophore community structure and
167 ancillary parameters were collected from a second CTD cast, while samples for detailed size
168 fractionated Chl *a* were collected from a third cast.

169 ### 2.2 Primary production

170 Carbon fixation rates were determined using the ^{13}C stable isotope method (Legendre and
171 Gosseline, 1996). Water samples (1.2 L) collected from the six irradiance depths were
172 inoculated with 45-46 µmol L^{-1} ^{13}C labelled sodium bicarbonate, representing 1.7-1.8 % of
173 the ambient dissolved inorganic carbon pool. Samples were incubated in an on-deck
174 incubator, chilled with sea surface water, and light depths were replicated using optical filters
175 (Misty-blue and Grey, LEE™). Incubations were terminated after 24 hours by filtration onto
176 pre-ashed (> 400 °C, > 4 hours) Whatman GF/F filters. Acid-labile carbon (PIC) was
177 removed by adding 1-2 drops of 1 % HCl to the filter followed by extensive rinsing with
178 freshly filtered (Fisherbrand MF300, ~0.7 µm pore size) unlabelled seawater. Filters were
179 oven dried (40°C, 8-12 hours) and stored in Millipore PetriSlides™. A parallel 55 % bottle

for size fractionated primary production (< 10 µm) was incubated alongside the other samples, with the incubation terminated by pre-filtration through 10-µm polycarbonate (Nuclepore™) filters and the filtrate was filtered and processed as above.

The isotopic analysis was performed on an Automated Nitrogen and Carbon Analysis prep system with a 20-20 Stable Isotope Analyser (PDZ Europa Scientific Instruments). The ^{13}C-carbon fixation rate was calculated using the equations described in Legendre and Gosseline (1996). The > 10-µm PP fraction was calculated as the difference between total PP and < 10-µm PP.

2.3 Community structure

Water samples for diatom and micro zooplankton counts, collected from predawn cast surface samples (5-15 m), were preserved with acidic Lugol's solution (2 % final solution) in 100-mL amber glass bottles. Cells were counted in 50 mL Hydro-Bios chambers using a Brunel SP-95-I inverted microscope (X200; Brunel Microscopes Ltd). Samples for flow cytometry were fixed with glutaraldehyde (0.5 % final solution) and stored at -80°C before being analysed using a FACS Calibur (Beckton Dickinson) flow cytometer (Zubkov et al., 2007).

Water samples (0.5-1 L) for coccolithophore cell numbers and species identification were collected from surface samples (5-15 m) onto cellulose nitrate filters (0.8-µm pore size, Whatman), oven dried and stored in Millipore PetriSlides™. Permanent slides of filter halves were prepared and analysed using polarizing light microscopy following Poulton et al. (2010). Coccolithophores were analysed to species level following Frada et al. (2010). For confirmation of species identification, a subset of filter halves were analysed by scanning electron microscope (SEM) following Daniels et al. (2012). Coccolithophore species were identified according to Young et al. (2003).

2.4 Chlorophyll *a*

Water samples (250 mL) for total Chl *a* analysis were filtered onto Fisherbrand MF300 filters. Parallel samples were filtered onto polycarbonate filters (10-µm) for > 10 µm Chl *a*. Samples for detailed size fractionated Chl *a*, collected in duplicate from a single depth in the upper water column (12-35 m), were filtered in parallel onto polycarbonate filters of various pore size (2, 10, 20-µm) and MF300 filters (effective pore size 0.7 µm). Filters were extracted in 8 mL of 90 % acetone (Sigma) for 20-24 hours (dark, 4°C). Measurements of

Chl *a* fluorescence were analysed on a Turner Designs Trilogy Fluorometer, calibrated using a solid standard and a chlorophyll *a* extract.

2.5 Ancillary parameters

Particulate inorganic carbon (PIC) measurements were made on water samples (500 mL) filtered onto polycarbonate filters (0.8 μm pore-size, Whatman), rinsed with trace ammonium solution (pH ~10) and oven-dried (6-8 hours, 30-40 °C). The analysis was carried out following Daniels et al. (2012) except that extractions were carried out in 5.0 mL of 0.4 mol L^{-1} nitric acid, erroneously reported as 0.5 mL in Daniels et al. (2012). Particulate silicate ($bSiO_2$) samples were collected onto polycarbonate filters (0.8 μm pore-size, Whatman), rinsed with trace ammonium solution (pH ~10) and oven-dried (6-8 hours, 30-40 °C). Digestion of $bSiO_2$ was carried out in polypropylene tubes using 0.2 mol L^{-1} sodium hydroxide, before being neutralised with 0.2 mol L^{-1} hydrochloric acid (Ragueneau and Tréguer, 1994; Brown et al., 2003). The solutions were analysed using a SEAL QuAAtro autoanalyser and no corrections were made for lithogenic silica. Macronutrients (nitrate, phosphate, silicic acid) concentrations were determined following Sanders et al. (2007) on a Skalar autoanalyser.

Samples for total dissolved inorganic carbon (C_T) were drawn into 500 ml borosilicate bottles. No filtering of samples occurred prior to analysis. Samples were stored in the dark and analysed within 12 hours of sampling, thus no poisoning was required. C_T was determined using coulometric titration (Johnson et al., 1987) with a precision of ≤ 2 μmol kg^{-1}. Measurements were calibrated against certified reference material (CRM, Dickson, 2010). Seawater pH_T was measured using the automated marine pH sensor (AMpS) system as described in Bellerby et al. (2002) modified for discrete mode. This system is an automated spectrophotometric pH sensor that makes dual measurements of thymol blue. The pH_T data used in this study were computed using the total hydrogen ion concentration scale and has a precision of 0.0002 pH_T and an estimated accuracy of better than 0.0025 pH_T units against CRM standards. The measured C_T and pH_T, with associated temperatures and salinity, were input to CO2SYS (Lewis and Wallace, 1998) to calculate saturation state of $CaCO_3$ using the dissociation constants for carbonic acid of Dickson and Millero (1987), boric acid from Dickson (1990b), sulphuric acid following Dickson (1990a) and the CO_2 solubility coefficients from Weiss (1974).

Satellite data on Chl *a*, photosynthetically available radiation (PAR) and sea surface temperature (SST) were obtained from the Aqua Moderate Resolution Image Spectroradiometer (MODIS) as 4 km resolution, 8 day composites. Data were extracted as averaged 3 x 3 pixel grids, centred on the sampling locations. Day length was calculated according to Kirk (1994). The R/V *Meteor* was not fitted with a PAR sensor, thus satellite measurements were the only available source of PAR data.

2.6 Data availability

Data included in the paper are available from the data repository PANGAEA via Daniels and Poulton (2013) for the measurements of primary production, chlorophyll *a*, particulate inorganic carbon and particulate silicate, cell counts of coccolithophores, diatoms and microzooplankton; Esposito and Martin (2013) for measurements of nutrients; Paulsen et al. (2014) for measurements of picoplankton and nanoplankton; and Bellerby (2014) for measurements of the carbonate chemistry.

3. Results

3.1 General oceanography

The two sites were characterised by very different water column profiles throughout the study period. In the NWB, a pycnocline persisted over the upper 400 m with a variable mixed layer (20 - 100 m, Fig. 2D). In contrast, the ICB appeared well mixed over the upper 400 m when considered over the equivalent density range (Fig. 2A). However, weak unstable stratification was observed in the upper 100 m when examined over a much narrower range in density (Fig. 2A inset).

Sea surface temperature (SST) showed little variation at both sites (Table 1), while the ICB (8.6 - 8.9 °C) was consistently warmer than the NWB (6.5 - 7.2 °C). Satellite estimates of SST were colder than in situ measurements and exhibited greater variability (Fig. 3A). However, the general pattern of the ICB being warmer than the NWB was observed from both in situ measurements and satellite derived ones. Sea -surface salinity (SSS), pH_T and Ω_{Ca} were relatively stable throughout the study with total ranges of 35.1 - 35.3, 8.0 - 8.1 and 3.0 - 3.2, respectively (Table 1).

Initial surface water concentrations of nitrate (NO_3) and phosphate (PO_4) were ~12 mmol N m^{-3} and ~0.7-0.8 mmol P m^{-3} at both sites (Table 1). Silicic acid (dSi) was high throughout the study period (mostly > 4 mmol Si m^{-3}), with slightly higher concentrations in the NWB

(5.3 - 5.7 mmol Si m^{-3}) than the ICB (< 5 mmol Si m^{-3}). Drawdown of 1 mmol m^{-3} of NO_3 and dSi occurred in the ICB between the 19th and 27th April, but then returned to previous levels by the 29th April. Nutrient drawdown did not occur in the NWB during the cruise period.

Both sites showed a similar trend of increasing daily PAR during the study (Fig. 3B); a twofold increase in the NWB (from 12.3 to 28.4 mol quanta m^{-2} d^{-1}) and a slightly smaller increase in the ICB (from 13.5 to 24.3 mol quanta m^{-2} d^{-1}). Daily irradiance continued to increase after the cruise finished, peaking around 40 - 45 days later at values in excess of 40 mol quanta m^{-2} d^{-1} (Fig. 3B). The general trend of increasing PAR was also reflected in the day length (Fig. 3B). At both sites, the euphotic depth shoaled as the study progressed, from 115 m to 50 m in the ICB and from 80 m to 56 m in the NWB (Table 2). However, the euphotic depth again deepened by 36 m between the 3rd and 4th visits to the ICB.

For the duration of the cruise until the 27th April (Day 118), surface and euphotic zone integrated particulate silicate ($bSiO_2$) increased in the ICB, peaking at 0.66 mmol Si m^{-3} and 37.1 mmol Si m^{-2}, respectively (Fig. 4A, Table 2), with a significant decline in $bSiO_2$ after this date. Lower values of $bSiO_2$, with little temporal variation, were found in the NWB, although a small increase in surface $bSiO_2$ was observed between the 14th and 22nd April (from 0.05 to 0.08 mmol Si m^{-3}, Fig. 4A). Standing stocks of PIC were less variable than $bSiO_2$. Highest surface values were observed during the last visit to the NWB (0.20 mmol C m^{-3}), while integrated calcite peaked at 11 mmol C m^{-2} on the 27th April in the ICB (Table 2).

3.2 Chlorophyll *a*

Profiles of CTD fluorescence in the NWB had a relatively consistent structure with high fluorescence in the stratified upper water column (Figs. 2E & 2F). Intra-site variation can be seen in the relative fluorescence values in surface waters, but a consistent increase over time was not observed. Fluorescence profiles in the ICB were more variable (Figs. 2B & 2C), ranging from profiles with high surface fluorescence (10th April, Day 101) to profiles with elevated fluorescence throughout the upper 300 m.

Acetone extracted measurements of chlorophyll *a* (Chl *a*) ranged from 0.1 to 2.3 mg m^{-3} with highest values generally in surface waters (5 - 15 m). Surface Chl *a* was variable in the ICB, with the lowest surface values (0.27 - 0.31 mg m^{-3}) measured during the first visit (Table 2). Peak Chl *a* values in the ICB occurred on the 10th April (2.2 mg m^{-3}), after which Chl *a* declined reaching a low of 0.62 mg m^{-3} by the end of the study (but remaining above initial

Chl *a* values). Initial surface Chl *a* values were higher in the NWB (0.58 mg m^{-3}) than the ICB, and generally increased throughout the cruise. However, the magnitude of this increase was significantly smaller than in the ICB, peaking at only 0.93 mg m^{-3}. Euphotic zone integrated Chl *a* showed a similar pattern to surface Chl *a* across both stations, with highest values on the 10th April (ICB, 146.4 mg m^{-2}).

Satellite estimates of Chl *a* also showed an increase in Chl *a* at both sites during the cruise (Figs. 3C & 3D), although these values (< 0.4 mg m^{-3}) were much lower than measured in situ Chl *a* (Table 2). The large increase in Chl *a* associated with North Atlantic spring blooms occurred between 20 and 30 days after the cruise (Figs. 3C & 3D). Both sites were characterised by two peaks in Chl *a* throughout the year, one in late spring (mid-June) and another in late summer (mid-August). The largest satellite-derived Chl *a* values occurred in the ICB in late spring (1.7 mg m^{-3}, Fig. 3C), while in the NWB, peak Chl *a* occurred during the late summer bloom (1.6 mg m^{-3}, Fig. 3D).

Size fractionated Chl *a* revealed very different communities at the two sites (Table 2 and Fig. 5). Initially in the ICB, approximately a quarter of the Chl *a* biomass was derived from the > 10 µm fraction (24 - 28 %; Table 2, Fig. 5A). On subsequent visits this increased significantly to 56 - 94 % (Table 2, Fig. 5A). A general trend of an increasing contribution from the > 10 µm fraction was also observed in those samples collected for more detailed size fractionation (Fig. 5C). The detailed size fractionation showed that excluding the first ICB visit where samples were not collected, the > 10 µm fraction was completely dominated by the > 20 µm fraction in the ICB (Fig. 5C). Conversely, the > 10 µm fraction formed only a minor component (< 21 %) of the Chl *a* biomass in the NWB, although the > 10 µm contribution did increase throughout the cruise (Table 2, Fig. 5B). Detailed size fractionation in the NWB showed that the biggest increase in contribution came from the 2-10 µm fraction, increasing from 14 % to 32 % (Fig. 5D), which was due to an increase in the absolute value of 2 - 10 µm Chl *a* (from 0.09 to 0.31 mg m^{-3}).

3.3 Primary production

Primary production (PP) in surface waters (5 - 15m) ranged from 0.41 to 4.89 mmol C m^{-3} d^{-1} in this study (Table 2), with PP generally decreasing with depth. Surface PP correlated well with euphotic zone integrated PP ($r = 0.98$, $p < 0.001$, $n = 7$). The largest change in PP occurred in the ICB, between the 26th March and the 10th April, when peak PP rates were observed in both the surface waters (4.89 mmol C m^{-3} d^{-1}) and integrated over the euphotic

zone (221.9 mmol C m^{-2} d^{-1}, Table 2). Following this peak, PP in the ICB declined, although it generally remained higher than pre-peak PP rates. The > 10 µm PP fraction contributed between 35 - 61 % of the total PP in the ICB. In contrast, the range and maximum rate of PP in the NWB was much lower than the ICB (0.67 - 1.11 mmol C m^{-3} d^{-1}, Table 2) with the > 10 µm PP making up a much smaller fraction (< 20 %). However, a clear increase in the > 10 µm PP fraction was observed between the 14th April (5 %) and the 25th April (20 %). The general trend in total and size-fractionated PP at both sites reflected that observed in the Chl *a* measurements.

3.4 Community structure

3.4.1 Community structure – picoplankton and nanoplankton

Flow cytometry identified *Synechococcus*, autotrophic picoeukaryotes and autotrophic nanoplankton (< 10 µm) in relatively high abundance in all samples (Table 3). In general, *Synechococcus* and picoeukaryotes were more abundant in the NWB than the ICB. In the NWB, a contrasting pattern between *Synechococcus,* nanoplankton and picoeukaryotes was observed; while *Synechococcus* and the nanoplankton increased significantly from 2,617 to 5,483 cells mL^{-1} and 484 to 1,384 cells mL^{-1} respectively, a large decrease in picoeukaryotes was also observed, from 18,016 to 8,456 cells mL^{-1}. A less coherent pattern was observed in the ICB, where peak concentrations of both *Synechococcus* (2,112 cells mL^{-1}) and picoeukaryotes (6,982 cells mL^{-1}) occurred on the 19th April, with a general decline after this date.

3.4.2 Community structure – coccolithophores

The coccolithophore species identified by polarised light microscopy were: *Emiliania huxleyi*, *Coccolithus pelagicus*, *Calcidiscus leptoporus*, *Coronosphaera mediterranea* and *Syracosphaera pulchra*. More detailed SEM observations found a number of other species at low cell densities not clearly identified by the light microscope: *Algirosphaera robusta*, *Acanthoica quattrospina*, *Calciopappus caudatus*, *Gephyrocapsa muellerae*, *Syracosphaera corolla*, *S. marginaporata, S. molischii, S. nodosa*, *S. ossa* and unidentified *Syracosphaera* spp. Many of these coccolithophore species have cell diameters between 10 and 20 µm, with the notable exceptions of *E. huxleyi*, *G. muellerae* and the smaller *Syracosphaera* spp. (Young et al., 2003). Two morphotypes of *E. huxleyi* were observed in all samples (A and B) with morphotype A consistently dominant (71 - 100 % of total *E. huxleyi* numbers). The

368 coccolithophore composition at both sites were similar, with *E. huxleyi* generally the most
369 abundant species (4.4 - 28.1 cells mL^{-1}, Table 3) at both sites, while *Coccolithus pelagicus*
370 was present in all samples at relatively low cell densities (0.15 - 2.79 cells mL^{-1}). The NWB
371 was also characterised by the presence of *A. robusta* (2.7 - 12.7 cells mL^{-1}), while *S.*
372 *marginaporata* (0 - 21.3 cells mL^{-1}) was only present in the ICB.

373 A general increase in coccolithophore abundance was observed in the ICB, with a large
374 increase between the 10th and 18th April (7.7 - 42.8 cells mL^{-1}). *Emiliania huxleyi* abundance
375 decreased between the 27th and 29th April (26.7 - 13.2 cells mL^{-1}), but *C. pelagicus* remained
376 relatively constant (0.81 - 0.84 cells mL^{-1}). In the NWB, coccolithophores generally followed
377 the trend of increasing Chl *a* with increases in abundance over time (Table 3). Within the
378 coccolithophore communities, the largest relative increase in species abundance was by *C.*
379 *pelagicus* with a sevenfold increase (0.38 to 2.66 cells mL^{-1}) between the 14th and 22nd of
380 April in the NWB.

381 ### 3.4.3 Community structure – diatoms and microzooplankton

382 The diatom taxa identified by light microscopy were: *Chaetoceros*, *Cylindrotheca*,
383 *Dactyliosolen*, *Guinardia*, *Leptocylindrus*, *Navicula*, *Pseudo-nitzschia*, *Rhizosolenia*,
384 *Thalassionema*, and *Thalassiosira.* Whilst samples for diatom counts were collected only
385 once per visit to each station, particulate silicate ($bSiO_2$) samples were collected from two
386 CTD casts per visit. As the major source of $bSiO_2$, the significant variability observed in
387 $bSiO_2$ between the two CTD casts at each visit (Fig. 4A) suggested a temporal variability in
388 the diatom cell abundance not captured in the Lugol's counts. Therefore, diatom abundance
389 counts were supplemented using SEM image based diatom counts from samples collected
390 from those CTDs where Lugol's samples were not collected (Fig. 4B). However, due to the
391 relatively smaller volumes examined by SEM (~ 4.2 mL versus 50 mL), there is a greater
392 inherent error in the counts and as such Lugol's counts were used wherever possible.

393 The diatom community was highly variable in the ICB (Fig. 4). Initially present only in very
394 low abundances (1.3 cells mL^{-1}, Table 3), a peak concentration of 249 cells mL^{-1} was reached
395 15 days later on the 10th April (Day 101). The population then decreased over the rest of the
396 study, down to 88 cells mL^{-1}, but remained above initial levels. A shift in composition was
397 observed after the population peaked, from a *Chaetoceros* dominated community (67 - 71 %)
398 on the 7th to 10th April (Days 98 to 101) to one dominated by *Pseudo-nitzschia* (65 - 73 %,
399 Fig. 4B) on the 27th to 29th April (Days 118 to 120). Diatoms were virtually absent from light

microscope measurements of the NWB, reaching a maximum of only 0.5 cells mL^{-1} (Table 3).

The main microzooplankton groups present were planktonic ciliates and small (~5 - 10 µm) naked dinoflagellates (e.g. *Gyrodinium* and *Gymnodinium*). Microzooplankton concentrations were ~ 4 times higher in the NWB (10.8 - 17.6 cells mL^{-1}, Table 3) than in the ICB (2.5 - 4.7 cells ml^{-1}, Table 3). Dinoflagellates initially dominated in the NWB (8.5 cells mL^{-1}), but were succeeded by ciliates (11.9 - 12.9 cells mL^{-1}). Both dinoflagellates and ciliates were present in similar concentrations in the ICB, except for the final visit, when dinoflagellates dominated (4.2 cells mL^{-1}).

4. Discussion

4.1 Time series or mixing?

The dynamic nature of the ocean causes inherent difficulties in interpreting data collected from fixed-point, Eulerian time-series, such as those in this study. The distribution of phytoplankton in the ocean exhibits significant heterogeneity, which can be driven by mesoscale physical processes (Martin, 2005). Therefore, Eulerian time-series are vulnerable to advection such that instead of repeatedly sampling the same phytoplankton community, each sample is potentially from a different population, possibly with a different composition. Before examining the development of the phytoplankton community, it is therefore necessary to consider the physicochemical environment. Eddies and other mesoscale features would potentially cause significant variations in measured SST, SSS, nutrients and carbonate chemistry. With the possible exception of the nutrient concentrations, which will also be affected by the biology present, the measured physicochemical parameters were stable throughout the study period (Table 1). Therefore, although we cannot rule out the influence of mesoscale features and advection during the study, the relative consistency of the sampled physicochemical environment suggests that the community structure is representative of the location, rather than from multiple eddies, and thus we can examine how the community developed during the cruise and compare between two geographically separated sites.

4.2 Drivers of the phytoplankton bloom

Density profiles in the Iceland Basin (ICB) were seemingly indicative of a well-mixed water column (Fig. 2A), yet elevated fluorescence in the upper 100 m of the water column suggests that phytoplankton cells were not being evenly mixed throughout the water column (Fig. 2B).

A detailed examination of the upper 100 m found small changes in the density profiles (Fig. 2A inset), corresponding to the elevated fluorescence, however the change in density with respective to depth was smaller ($\Delta\sigma_t < 0.025$ over 1 m) than most metrics used to identify mixed layers (e.g. Kara et al., 2000). Elevated fluorescence with only minimal stratification is consistent with the critical turbulence hypothesis (Huisman et al., 1999); here it is likely that active mixing had ceased, allowing phytoplankton net growth, while the response of the physical environment was slower than the biological response, and stratification was only just beginning to develop.

Although ICB upper water column fluorescence was elevated throughout the study, there was significant variation in the magnitude and structure of the fluorescence profiles (Figs. 3B & 3C), as well as a peak and decline in surface chlorophyll *a* (Chl *a*) and primary production (PP). The general theory of bloom formation is that once conditions are favourable for bloom formation, the pre-bloom winter ecosystem will transition into a blooming ecosystem, identifiable by increasing Chl *a* biomass and PP. However, we did not observe this smooth transition. Instead we observed periods of stability, characterised by increased stratification, Chl *a* and PP, followed by periods of instability where increased mixing weakened the developing stratification. Increased mixing detrains phytoplankton out of the surface waters, reducing both Chl *a* biomass and PP, and exporting them to depth (Giering et al., *in review*). One such mixing event occurred between the 27th and 29th April (Days 118 and 120), where minor stratification ($\Delta\sigma t = 0.019$) disappeared ($\Delta\sigma t < 0.001$) over the upper 25 m, surface Chl *a* halved from 1.18 mg m^{-3} to 0.62 mg m^{-3}, and the fluorescence profile became well-mixed (Fig. 2C). Furthermore, surface nutrients were replenished (Table 1), all of which are indicative of a mixing event.

The transition period from winter to spring was also observed in satellite data from the ICB. Bloom metrics (Siegel et al., 2002; Henson et al., 2009) of satellite Chl *a* estimate that the main spring bloom did not begin until ~ 20 days after our study period (dashed line in Fig. 3C). However, there was a significant increase ($r = 0.99$, $p < 0.015$, $n = 4$) in Chl *a* during the study period (Fig. 3C inset), consistent with our in situ observations, that suggests that while the environment was not yet stable enough for sustained and rapid phytoplankton growth, intermittent net phytoplankton growth did occur. Therefore, we suggest that the early stages of a spring bloom are characterised by periods of instability and net growth, and that rather than a single smooth transition into a bloom, for a period of weeks prior to the main spring bloom event, phytoplankton form temporary mini-blooms during transient periods of

stability. The export flux from these pre-bloom communities is a potentially significant food source to the mesopelagic (Giering et al., *in review*).

In contrast to the instability of the ICB, the Norwegian Basin (NWB) was relatively stable with a strong and persistent pycnocline (Fig. 2D), as well as elevated fluorescence in the upper mixed layer (Fig. 2E). However, a variable mixed layer that did not consistently shallow in the NWB (Fig. 2D) suggests variability in the strength of the physical forcing, that may explain why although Chl *a* and PP increased throughout the cruise, they remained below that observed in the ICB during the study period (Table 2). Furthermore, the net community growth rate (Chl *a* derived, μ_{Chl}), was relatively low (0.02 d^{-1}), suggesting that as was the case for the ICB, the main spring bloom was yet to start. This was also confirmed from the satellite Chl *a,* which showed a very similar pattern to the ICB: although Chl *a* increased during our study period (Fig. 3D inset), the main bloom did not start until ~ 20 days later (Fig. 3D). Therefore despite very different physical environments, the two sites both represented early stages in the development of spring blooms.

Unlike the ICB, the factors limiting bloom formation in the NWB cannot easily be attributed to the physicochemical environment. A switch from negative to positive net heat flux has been linked to spring bloom formation (Taylor and Ferrari, 2011b; Smyth et al., 2014), but here the net heat flux was negative for the majority of the study at both sites (C. Lindemann, pers. comm., Giering et al., *in review*). Irradiance is a key driver of phytoplankton growth and bloom formation; the main spring bloom did not occur until daily PAR reached its seasonal maximum of 45 mol photons m^{-2} d^{-1} (Figs. 3B, 3C & 3D). The general increase in daily PAR over our study period was coupled with an increase in Chl *a* and PP in the NWB, suggesting that despite a stratified environment, irradiance was an important driving factor. Although the magnitude of the daily flux of PAR at both sites was similar, Chl *a* and PP were higher in the less stable ICB than the NWB, suggesting that irradiance was not the only driver of the NWB phytoplankton community. Irradiance levels can also have a secondary influence on the requirements for phytoplankton growth. While macronutrients were replete at both sites, we did not measure micronutrients such as iron (Fe). The cellular Fe demand increases in low light conditions (Moore et al., 2006), and as such Fe may be limiting at this early stage of bloom formation in the Norwegian Basin. However, without measurements of Fe (or phytoplankton photophysiology), we cannot directly test this hypothesis. Although temperature limits phytoplankton gross growth rates (Eppley, 1972), the relatively small

difference in temperature between the NWB and the ICB (~1.5 - 2.5 °C) is unlikely to have a significant impact on gross growth rates (Eppley, 1972).

Besides physicochemical drivers of bloom formation, the plankton community itself can play a large role in the development and formation of a bloom. Physiological parameters such as net growth rates (μ_{Chl}) and 'assimilation efficiency' (i.e. PP normalised to biomass, in this case Chl *a*) can provide an insight into the state of the phytoplankton community. The NWB community had a noticeably lower assimilation efficiency (13.5 - 15.8 g C [g Chl *a*]$^{-1}$ d^{-1}) than that in the ICB (15.7 - 27.0 g C [g Chl *a*]$^{-1}$ d^{-1}), thus the relative increase in biomass in the NWB was slower, as reflected in the growth rates where the maximum estimated (net) growth rate in the NWB (μ_{Chl} = 0.05 d^{-1}) was much lower than in the ICB (μ_{Chl} = 0.22 d^{-1}). Assimilation efficiency varies with both environmental conditions and species composition, and therefore the composition of the phytoplankton community is likely to be another key driver behind the contrasting phytoplankton dynamics observed in the ICB and NWB.

4.3 Overall community composition

The contrasting structures of Chl *a* and PP size fractions observed at the two sites (Fig. 5, Table 2), were reflected in the contrasting composition of the phytoplankton communities (Table 3). In the ICB, a change in dominance in both Chl *a* and PP, from < 10 µm to the > 10 µm fraction, occurred as the diatom abundance increased between the 26th March and the 7th April. An increase in the abundance of the < 10 µm community was also observed during this period, composed mainly of < 2 µm *Synechococcus* and pico-eukaryotes (Table 3, Fig. 5C). However, with most of the diatom population having cells > 20 µm (Fig. 5C), their relatively large size allowed the diatoms to dominate both the Chl *a* and PP while remaining numerically inferior. The decline in total Chl *a* and PP later in our study was reflected by a decreasing abundance of most of the phytoplankton community (Table 3). However, the relative decrease of pico-phytoplankton (*Synechococcus* and picoeukaryotes) was greater than that of the diatoms, such that the > 10 µm fraction increased its dominance for both Chl *a* (94 %) and PP (61 %). Therefore, although surface Chl *a* and PP declined after the 'mini-bloom event' which peaked around the 10th April, the community structure did not return to a pre-bloom composition, but instead remained dominated by diatoms.

Interestingly, the phytoplankton response to the increased diatom abundance was not uniform, with the nanoplankton abundance decreasing and *Synechococcus* increasing only after the peak in diatom abundance. Thus, we observed that the phytoplankton community

response during the spring bloom was not universal across functional types as has been previously observed elsewhere (Brown et al., 2008).

In contrast to the ICB, a large shift in the NWB community was not observed. Pico-eukaryotes dominated both in terms of abundance (Table 3) and Chl *a*, through the < 2 µm fraction (Fig. 5D). This is consistent with previous observations of early stage spring blooms (Joint et al., 1993). Although the < 2 µm Chl *a* fraction showed little variation throughout the study (0.45 - 0.58 mg m^{-3}), variation in the < 2 µm phytoplankton composition did occur, with an apparent succession from pico-eukaryotes to *Synechococcus* and nanoplankton. This may represent a community shift early in development of the spring bloom or may demonstrate the inherent variability within pre-bloom communities.

The increase in total Chl *a* in the NWB was driven primarily by the 2 to 10 µm fraction, which was likely composed of the nanoplankton, which itself had a threefold increase in population size (from 484 to 1384 cells mL^{-1}, Table 3). The phytoplankton responsible for the observed increase in the >10 µm Chl *a* and PP fraction cannot be confidently determined; large diatoms were absent and thus could not contribute. The microzooplankton population consisted of ciliates and dinoflagellates (*Gyrodinium* and *Gymnodinium*), both of which have been reported to be mixotrophic (Putt, 1990; Stoecker, 1999), and thus could potentially have contributed to the Chl *a* measurements. Furthermore, it is possible that part of the nanoplankton community, as measured by flow cytometry, was > 10 µm and thus the increasing concentration of nanoplankton could also contribute to the increase in the > 10 µm fraction.

4.4 Relative independence of the coccolithophore community

The traditional view on the seasonality of coccolithophores is that they succeed the diatom spring bloom, forming coccolithophore blooms in late summer. However, here we observed a typical North Atlantic community of coccolithophores (Savidge et al., 1995; Dale et al., 1999; Poulton et al., 2010), growing alongside the ICB diatom bloom, rather than just succeeding the diatoms. This is consistent with the “rising tide” hypothesis of Barber and Hiscock (2006), as well as observations from both in situ (Leblanc et al., 2009) and satellite measurements (Hopkins et al., in review) suggesting that coccolithophores are present in North Atlantic spring blooms. Despite the contrasting environment and overall community structure of the NWB, the coccolithophore dynamics were similar, appearing independent of the overall community dynamics. Species-specific growth rates of coccolithophores

(calculated from changes in cell concentration) found that *E. huxleyi* had the same net growth rate at both sites ($\mu = 0.06\ d^{-1}$), while the net growth rate of *C. pelagicus* was comparable to *E. huxleyi* in the ICB, but was slightly higher in the NWB ($\mu = 0.13\ d^{-1}$). Culture experiments of *E. huxleyi* and *C. pelagicus* have found comparable gross growth rates at temperatures below 10 °C (Daniels et al., 2014), and our in situ observations support this conclusion. That *C. pelagicus* has higher net growth rates could also be indicative of higher grazing on the relatively smaller *E. huxleyi* (Daniels et al., 2014).

4.5 Contrasting patterns of diatoms

The diatom bloom in the ICB, which began between the 26th March (Day 86) and the 7th April (Day 98), was initially dominated by *Chaetoceros* (71 - 67 % of total cell numbers, Fig. 4B). As the community developed however, *Pseudo-nitzschia* succeeded as the dominant diatom genera (65 - 73 % of total). Both *Chaetoceros* and *Pseudo-nitzschia* are common spring bloom diatoms (Sieracki et al., 1993; Rees et al., 1999; Brown et al., 2003), with *Chaetoceros* often dominant in the earlier stages of North Atlantic spring blooms (Sieracki et al., 1993; Rees et al., 1999). Resting spores of *Chaetoceros* have also been observed to dominate the export flux out of the Iceland Basin during the North Atlantic spring bloom in May 2008 (Rynearson et al., 2013), suggesting dominance of the spring bloom prior to this period, consistent with the early community observed in our study.

Pseudo-nitzschia (previously identified as *Nitzschia* in other studies), tends to dominate later in the spring bloom (Sieracki et al., 1993; Moore et al., 2005), also consistent with this study. This suggests that as a genera, *Chaetoceros* are either able to adapt more quickly than *Pseudo-nitzschia*, or that they have a wider niche of growing conditions through a large diversity of species. However, once established, *Pseudo-nitzschia* are able to outcompete *Chaetoceros*, resulting in a community shift. That the succession of the diatom community observed in the ICB is consistent with that expected in the main diatom spring bloom, suggests that a mini-diatom bloom occurred prior to the formation of the main spring bloom.

The observed variability in the relationship between diatoms (the main source of $bSiO_2$) and $bSiO_2$ was likely due to the species-specific variability in the cellular $bSiO_2$ content of diatoms (Baines et al., 2010). The abundance of *Pseudo-nitzschia*, rather than *Chaetoceros*, best explained the trend in $bSiO_2$ ($r = 0.92$, $p < 0.001$, $n = 8$), suggesting that *Pseudo-nitzschia* was the major producer of $bSiO_2$. Previously *Chaetoceros* has been observed as the

591 major exporter of $bSiO_2$ in the Iceland Basin (Rynearson et al., 2013). Here, as the major
592 producer of $bSiO_2$, *Pseudo-nitzschia* has the potential to also be the major exporter of $bSiO_2$.

593 In contrast to the ICB, diatoms appeared to be virtually absent (< 0.5 cells mL^{-1}) in the NWB.
594 While the dSi:NO_3 ratio was below the 1:1 requirement for diatoms, consistent with previous
595 studies of North Atlantic blooms (Leblanc et al., 2009), dSi did not become depleted (always
596 above 5 mmol Si m^{-3}, Table 1) and thus was not limiting. Furthermore, significant and
597 increasing concentrations of particulate silicate ($bSiO_2$) were measured throughout the cruise
598 (Fig. 4A). As the main source of $bSiO_2$, diatoms would therefore be expected to be present.
599 Although absent in the Lugol's counts, examination of SEM images found significant
600 numbers (101 - 600 cells mL^{-1}) of small (< 5 µm) diatoms (predominantly *Minidiscus* spp.)
601 that were too small to be identified by light microscopy. However, they may still constitute
602 an important component of the nanoplankton, as measured by flow cytometry. As a result of
603 their small cell size, nano-sized diatoms, such as *Minidiscus*, are easily missed when
604 identifying and enumerating the phytoplankton community, and as such their potential
605 biogeochemical importance may be greatly underestimated (Hinz et al., 2012). Other nano-
606 sized diatom species have been observed as major components of the phytoplankton
607 community on the Patagonian Shelf (Poulton et al., 2013), in the Scotia Sea (Hinz et al.,
608 2012), the northeast Atlantic (Boyd and Newton, 1995; Savidge et al., 1995) and in the
609 Norwegian Sea (Dale et al., 1999).

610 The *Minidiscus* spp. observed in this study exhibited a significant increase in population size
611 during the study, from initial concentrations of 100 to 200 cells mL^{-1}, then up to 600 cells
612 mL^{-1} by the end of the study, and correlating well with both $bSiO_2$ ($r = 0.93$, $p < 0.01$, $n = 6$),
613 and Chl *a* ($r = 0.93$, $p < 0.01$, $n = 6$). Furthermore, the increasing concentration of
614 *Minidiscus* corresponded to the increase in the 2 to 10 µm Chl *a* size fraction (Fig. 5D). The
615 maximum net growth rate of *Minidiscus*, estimated from changes in cell abundances (μ =
616 0.13 d^{-1}), was significantly higher than that calculated for the total community using Chl *a*
617 ($\mu_{Chl} = 0.05\ d^{-1}$). While different methods were used to determine these growth rates, it does
618 suggest that conditions were favourable for the small nano-sized diatoms to grow more
619 rapidly than the bulk community.

620 The question therefore remains as to why the larger (> 10 µm) diatoms were virtually absent
621 in an environment that is physically stable and nutrient replete, while small diatoms were able
622 to thrive? The fate and ecology of overwintering oceanic diatoms is poorly understood. Many
623 diatom species, both neritic and pelagic, are capable of forming resting stages that sink post

bloom (Smetacek, 1985; Rynearson et al., 2013), yet diatoms must be present in spring when the diatom bloom begins. Therefore, either a diatom population is sustained in the upper water column over winter (Backhaus et al., 2003), or the spring diatom community is sourced from elsewhere (horizontally or vertically). In relatively shallow coastal environments, benthic resting stages overwinter until spring when they are remixed up into the water column, providing the seed population for the spring bloom (McQuoid and Godhe, 2004). It is unlikely that oceanic diatom blooms are seeded from the sediment, as the depths are far too great for remixing. However, viable diatom cells have been observed suspended at depth (> 1000 m) in the ocean (Smetacek, 1985), and it is possible that these suspended deep populations are remixed to seed the spring bloom. An alternative hypothesis is based on the observation that diatom blooms generally occur first in coastal waters before progressing to the open ocean (Smetacek, 1985), suggesting that coastal diatom populations are horizontally advected into pelagic waters, thus seeding the spring bloom in the open ocean from shelf waters. The location of the source coastal populations, and their transit time to the open ocean location, would then affect the timing of the diatom blooms

With such low concentrations of > 10 µm diatoms (< 0.5 cells mL^{-1}) in the NWB, it is possible that the overwintering diatom population was too small to seed the spring bloom. Grazing pressure by microzooplankton and mesozooplankton may influence the composition and timing of the onset of the spring bloom (Behrenfeld and Boss, 2014). The potential grazing pressure from the significant microzooplankton population (10.8 - 17.6 cells mL^{-1}) in the NWB may have exerted such a control on the observed diatom population that it could not develop into a diatom bloom. Instead an alternative seed population of diatoms may be required to overcome the grazing pressure and initiate the diatom bloom in the NWB. Whether the absence of large diatoms is a regular occurrence in the NWB, or whether inter-annual shifts between small and large diatoms occur, as observed in the northeast Atlantic (Boyd and Newton, 1995), will have significant implications for export and the functioning of the biological carbon pump. The absence of larger diatoms in pelagic spring blooms in the Norwegian Sea has also been observed by Dale et al. (1999), and it may be that large diatoms are completely absent from the pelagic south east Norwegian Sea. The lack of large diatoms in the NWB could explain the seasonal profile of satellite Chl *a* (Fig. 3D); with no large diatoms present, the spring bloom is less intense, peaking at only ~60 % of the Chl *a* concentration found in the ICB.

Clearly, further work is required to examine why large diatoms are absent from the initial stages of the spring bloom in the NWB, and whether they ever become abundant in this region.

5. Conclusions

During March-May 2012, satellite and in situ data from study sites in the Iceland Basin (ICB) and the Norwegian Basin (NWB) suggested that despite very different physical environments, the two sites both represented early stages in the development of the North Atlantic spring bloom. Spring bloom initiation in the ICB was limited by the physical environment, with periods of increased mixing inhibiting bloom formation. The physicochemical environment alone was not limiting bloom formation in the NWB as, in spite of a stable stratified water column and ample nutrients, Chl *a* biomass and primary production were relatively low. Phytoplankton efficiency (Chl *a* -normalised primary production) was also lower in the NWB, suggesting that the phytoplankton community composition and/or physiology was also a limiting factor in bloom formation.

The phytoplankton community in the NWB was dominated by the < 2 µm Chl *a* fraction, with high concentrations of pico-eukaryotes (~18,000 cells mL^{-1}) succeeded by *Synechococcus* and nanoplankton. In contrast, although the initial dominance of the < 10 µm Chl *a* fraction (pico-eukaryotes and nanoplankton) was succeeded by diatoms dominating in the > 10 µm Chl *a* fraction, the ICB phytoplankton community generally followed the "rising tide" hypothesis, with most of the community positively responding to the onset of the diatom bloom. Interestingly, coccolithophore dynamics were similar at both sites, independent of the overall community, with similar concentrations of the main species *Emiliania huxleyi* and *Coccolithus pelagicus*.

In terms of the diatom community, *Chaetoceros* initially dominated the ICB diatom bloom, but was replaced by *Pseudo-nitzschia* as the bloom progressed, suggesting *Chaetoceros* as a key species in diatom bloom formation, while *Pseudo-nitzschia* was the major source of particulate silicate ($bSiO_2$). The lack of large (> 10 µm) bloom forming diatoms in the NWB, while small (< 5 µm) diatoms were present in high numbers (101 - 600 cells mL^{-1}), suggests that micro-zooplankton grazing, coupled with a potential lack of a seed population, was restricting diatom growth in the NWB, or that large diatoms are absent in NWB spring blooms.

These results suggest that despite both phytoplankton communities being in the early stage of bloom formation and exhibiting positive net growth rates, different physicochemical and biological factors control bloom formation with the resulting blooms likely to be significantly different in terms of biogeochemistry and trophic interactions throughout the growth season. Clearly, more in situ studies are needed in the transitional period between winter and the peak productivity of the spring bloom to examine compositional differences, growth and mortality factors, and how regional variability impacts on upper ocean biogeochemistry and deep-sea fluxes of organic material. Coupled studies of satellite derived products, including bloom phenology and phytoplankton physiology, and in situ processes are needed to examine the full spectrum of factors forming the spring bloom.

Acknowledgements

The 'Deep Convection' cruise was funded by the Deutsche Forschunggemeinschaft in a grant to M.S.J with financial support for this research from the EU Framework 7 EuroBASIN (EUROpean Basin-scale Analysis, Synthesis & Integration) project. C.J.D had additional financial support from the UK Natural Environmental Research Council, via a Studentship, A.J.P and A.P.M were also supported by NERC National Capability funding. We thank the officers and crew of the R/V Meteor; Gisle Nondal, Emanuele Reggiani, Emil Jeansson and Tor de Lange for the measurements of carbonate chemistry parameters; Theresa Reichelt for running and processing the CTD data; Mark Stinchcombe for $bSiO_2$ and nutrient measurements; Darryl Green and Matt Cooper for ICP-OES analyses; Stuart Painter, Keith Davidson and Sharon McNeill for ^{13}C and POC analyses; and Jason Hopkins for assistance with satellite data. Further thanks go to Stephanie Henson for her helpful comments on an early version of the paper. MODIS Aqua data were obtained from the NASA Ocean Color distributed archive (http://oceancolor.gsfc.nasa.gov/).

References

Backhaus, J. O., Hegseth, E. N., Wehde, H., Irigoien, X., Hatten, K., and Logemann, K.: Convection and primary production in winter, Mar. Ecol.-Prog. Ser., 251, 1-14, doi:10.3354/meps251001, 2003.

Baines, S. B., Twining, B. S., Brzezinski, M. A., Nelson, D. M., and Fisher, N. S.: Causes and biogeochemical implications of regional differences in silicification of marine diatoms, Global Biogeochem. Cy., 24, GB4031, doi:10.1029/2010GB003856, 2010.

Barber, R. T. and Hiscock, M. R.: A rising tide lifts all phytoplankton: Growth response of other phytoplankton taxa in diatom-dominated blooms, Global Biogeochem. Cy., 20, GB4S03, doi:10.1029/2006gb002726, 2006.

Behrenfeld, M. J.: Abandoning Sverdrup's Critical Depth Hypothesis on phytoplankton blooms, Ecology, 91, 977-989, doi:10.1890/09-1207.1, 2010.

Behrenfeld, M. J. and Boss, E. S.: Resurrecting the ecological underpinnings of ocean plankton blooms, Annu. Rev. Mar. Sci., 6, 167-194, doi:10.1146/annurev-marine-052913-021325, 2014.

Bellerby, R., Olsen, A., Johannessen, T., and Croot, P.: A high precision continuous spectrophotometric method for seawater pH measurements: The automated marine pH sensor (AMpS), Talanta, 56, 61-69, doi:10.1016/S0039-9140(01)00541-0, 2002.

Bellerby, R. G. J.: Discrete carbonate chemistry measured during the M87/1 cruise in April 2012, PANGAEA, doi:http://doi.pangaea.de/10.1594/PANGAEA.830294, 2014.

Boyd, P. and Newton, P.: Evidence of the potential influence of planktonic community structure on the interannual variability of particulate organic carbon flux, Deep-Sea Res Pt I, 42, 619-639, doi:10.1016/0967-0637(95)00017-Z, 1995.

Brody, S. R. and Lozier, M. S.: Changes in dominant mixing length scales as a driver of subpolar phytoplankton bloom initiation in the North Atlantic, Geophys. Res. Lett., 41, 3197-3203, doi:10.1002/2014GL059707, 2014.

738 Brown, L., Sanders, R., Savidge, G., and Lucas, C. H.: The uptake of silica during the spring
739 bloom in the Northeast Atlantic Ocean, Limnol. Oceanogr., 48, 1831-1845,
740 doi:10.4319/lo.2003.48.5.1831, 2003.

741 Brown, S. L., Landry, M. R., Selph, K. E., Jin Yang, E., Rii, Y. M., and Bidigare, R. R.:
742 Diatoms in the desert: Plankton community response to a mesoscale eddy in the
743 subtropical North Pacific, Deep-Sea Res. Pt. II, 55, 1321-1333,
744 doi:10.1016/j.dsr2.2008.02.012, 2008.

745 Dale, T., Rey, F., and Heimdal, B. R.: Seasonal development of phytoplankton at a high
746 latitude oceanic site, Sarsia, 84, 419-435, doi:10.1080/00364827.1999.10807347, 1999.

747 Daniels, C. J. and Poulton, A. J.: Chlorophyll-a, primary production rates, carbon
748 concentrations and cell counts of coccolithophores, diatoms and microzooplankton
749 measured in water samples from the North Atlantic during the M87/1 cruise in April 2012,
750 PANGAEA, doi:http://doi.pangaea.de/10.1594/PANGAEA.823595, 2013.

751 Daniels, C. J., Sheward, R. M., and Poulton, A. J.: Biogeochemical implications of
752 comparative growth rates of *Emiliania huxleyi* and *Coccolithus* species, Biogeosciences,
753 11, 6915-6925, doi:10.5194/bg-11-6915-2014, 2014.

754 Daniels, C. J., Tyrrell, T., Poulton, A. J., and Pettit, L.: The influence of lithogenic material
755 on particulate inorganic carbon measurements of coccolithophores in the Bay of Biscay,
756 Limnol. Oceanogr., 57, 145-153, doi:10.4319/lo.2012.57.1.0145, 2012.

757 Dickson, A. G.: Standard potential of the reaction: $AgCl(s) + 1/2H_2(g) = Ag(s) + HCl(aq)$,
758 and the standard acidity constant of the ion HSO_4^- in synthetic seawater from 273.15 to
759 318.15 K, J. Chem. Thermodyn., 22, 113-127, doi:10.1016/0021-9614(90)90074-Z,
760 1990a.

761 Dickson, A. G.: Standards for ocean measurements, Oceanography, 23, 34-47,
762 doi:10.5670/oceanog.2010.22, 2010.

763 Dickson, A. G.: Thermodynamics of the dissociation of boric acid in synthetic sea water from
764 273.15 to 318.15 K, Deep-Sea Res., 37, 755-766, doi:10.1016/0198-0149(90)90004-F,
765 1990b.

766 Dickson, A. G. and Millero, F. J.: A comparison of the equilibrium constants for the
767 dissociation of carbonic acid in seawater media, Deep-Sea Res., 34, 1733-1743,
768 doi:10.1016/0198-0149(87)90021-5, 1987.

769 Eilertsen, H. C.: Spring blooms and stratification, Nature, 363, 24-24, doi:10.1038/363024a0,
770 1993.

771 Eppley, R. W.: Temperature and phytoplankton growth in the sea, Fish. Bull., 70, 1063-1085,
772 1972.

773 Esposito, M. and Martin, A. P.: Nutrient concentrations of water samples collected by CTD-
774 rosettes during the cruise M87/1 in April 2012, PANGAEA,
775 doi:10.1594/PANGAEA.823681, 2013.

776 Fischer, A. D., Moberg, E. A., Alexander, H., Brownlee, E. F., Hunter-Cevera, K. R., Pitz, K.
777 J., Rosengard, S. Z., and Sosik, H. M.: Sixty years of Sverdrup: A retrospective of
778 progress in the study of phytoplankton blooms, Oceanography, 27, 222-235,
779 doi:10.5670/oceanog.2014.26, 2014.

780 Frada, M., Young, J. R., Cachao, M., Lino, S., Martins, A., Narciso, A., Probert, I., and de
781 Vargas, C.: A guide to extant coccolithophores (Calcihaptophycidae, Haptophyta) using
782 light microscopy, J. Nannoplankt. Res., 31, 58-112, 2010.

783 Giering, S. L. C., Sanders, R., Martin, A. P., Lindemann, C., Daniels, C. J., Mayor, D. J., and
784 St. John, M. A.: High export via small particles before the onset of the North Atlantic
785 spring bloom, Global Biogeochem. Cy., *in review*.

786 Henson, S. A., Dunne, J. P., and Sarmiento, J. L.: Decadal variability in North Atlantic
787 phytoplankton blooms, J. Geophys. Res., 114, C04013, doi:10.1029/2008JC005139, 2009.

788 Hinz, D. J., Poulton, A. J., Nielsdóttir, M. C., Steigenberger, S., Korb, R. E., Achterberg, E.
789 P., and Bibby, T. S.: Comparative seasonal biogeography of mineralising nannoplankton
790 in the scotia sea: *Emiliania huxleyi*, *Fragilariopsis* spp. and *Tetraparma pelagica*, Deep-
791 Sea Res. Pt. II, 59–60, 57-66, doi:10.1016/j.dsr2.2011.09.002, 2012.

792 Hopkins, J., Henson, S. A., Painter, S. C., Tyrrell, T., and Poulton, A. J.: Phenological
793 characteristics of global coccolithophore blooms, Global Biogeochem. Cy., 29, 239-253,
794 doi:10.1002/2014GB004919, 2015.

795 Huisman, J., van Oostveen, P., and Weissing, F. J.: Critical depth and critical turbulence:
796 Two different mechanisms for the development of phytoplankton blooms, Limnol.
797 Oceanogr., 44, 1781-1787, doi:10.4319/lo.1999.44.7.1781, 1999.

798 Johnson, K. M., Sieburth, J. M., Williams, P. J., and Brandström, L.: Coulometric total
799 carbon analysis for marine studies: Automation and calibration, Mar. Chem., 21, 117-133,
800 doi:10.1016/0304-4203(93)90201-X, 1987.

801 Joint, I., Pomroy, A., Savidge, G., and Boyd, P.: Size-fractionated primary productivity in the
802 northeast Atlantic in May–July 1989, Deep-Sea Res. Pt. II, 40, 423-440,
803 doi:10.1016/0967-0645(93)90025-i, 1993.

804 Kara, A. B., Rochford, P. A., and Hurlburt, H. E.: An optimal definition for ocean mixed
805 layer depth, J. Geophys. Res.-Oceans, 105, 16803-16821, doi:10.1029/2000JC900072,
806 2000.

807 Kirk, J. T. O.: Light and photosynthesis in aquatic ecosystems, Cambridge University Press,
808 Cambridge, 1994.

809 Leblanc, K., Hare, C. E., Feng, Y., Berg, G. M., DiTullio, G. R., Neeley, A., Benner, I.,
810 Sprengel, C., Beck, A., Sanudo-Wilhelmy, S. A., Passow, U., Klinck, K., Rowe, J. M.,
811 Wilhelm, S. W., Brown, C. W., and Hutchins, D. A.: Distribution of calcifying and
812 silicifying phytoplankton in relation to environmental and biogeochemical parameters
813 during the late stages of the 2005 North East Atlantic Spring Bloom, Biogeosciences, 6,
814 2155-2179, doi:10.5194/bg-6-2155-2009, 2009.

815 Legendre, L. and Gosseline, M.: Estimation of N and C uptake rates by phytoplankton using
816 ^{15}N or ^{13}C: revisiting the usual computation formulae, J Plankton Res, 19, 263-271,
817 doi:10.1093/plankt/19.2.263, 1996.

818 Lewis, E. and Wallace, D. W. R.: Program developed for CO_2 system calculations.
819 ORNL/CDIAC-105. Carbon Dioxide Information Analysis Center, O. R. N. L., U.S.
820 Department of Energy, Oak Ridge, Tennessee (Ed.), 1998.

821 Lindemann, C. and St. John, M. A.: A seasonal diary of phytoplankton in the North Atlantic,
822 Front. Mar. Sci., 1, 37, doi:10.3389/fmars.2014.00037, 2014.

823 Lochte, K., Ducklow, H. W., Fasham, M. J. R., and Stienen, C.: Plankton succession and
824 carbon cycling at 47°N 20°W during the JGOFS North Atlantic Bloom Experiment, Deep-
825 Sea Res. Pt. II, 40, 91-114, doi:10.1016/0967-0645(93)90008-b, 1993.

826 Mahadevan, A., D'Asaro, E., Lee, C., and Perry, M. J.: Eddy-driven stratification initiates
827 North Atlantic spring phytoplankton blooms, Science, 337, 54-58,
828 doi:10.1126/science.1218740, 2012.

829 Margalef, R.: Life-forms of phytoplankton as survival alternatives in an unstable
830 environment, Oceanol. Acta, 1, 493-509, 1978.

831 Martin, A.: The kaleidoscope ocean, Philos. T. Roy. Soc. A, 363, 2873-2890,
832 doi:10.1098/rsta.2005.1663, 2005.

833 McQuoid, M. R. and Godhe, A.: Recruitment of coastal planktonic diatoms from benthic
834 versus pelagic cells: Variations in bloom development and species composition, Limnol.
835 Oceanogr., 49, 1123-1133, doi:10.4319/lo.2004.49.4.1123, 2004.

836 Miller, C. B.: Biological Oceanography, Wiley-Blackwell, Oxford, 2003.

837 Moore, C. M., Lucas, M. I., Sanders, R., and Davidson, R.: Basin-scale variability of
838 phytoplankton bio-optical characteristics in relation to bloom state and community
839 structure in the Northeast Atlantic, Deep-Sea Res Pt I, 52, 401-419,
840 doi:10.1016/j.dsr.2004.09.003, 2005.

841 Moore, C. M., Mills, M. M., Milne, A., Langlois, R., Achterberg, E. P., Lochte, K., Geider,
842 R. J., and La Roche, J.: Iron limits primary productivity during spring bloom development
843 in the central North Atlantic, Glob. Change. Bio., 12, 626-634, doi:10.1111/j.1365-
844 2486.2006.01122.x, 2006.

845 Paulsen, M. L., Riisgaard, K., and Nielsen, T. G.: Abundance of pico- and
846 nanophytoplankton during the Meteor cruise M87/1, PANGAEA,
847 doi:http://doi.pangaea.de/10.1594/PANGAEA.839416, 2014.

Poulton, A. J., Charalampopoulou, A., Young, J. R., Tarran, G. A., Lucas, M. I., and Quartly, G. D.: Coccolithophore dynamics in non-bloom conditions during late summer in the central Iceland Basin (July–August 2007), Limnol. Oceanogr., 55, 1601-1613, doi:10.4319/lo.2010.55.4.1601, 2010.

Poulton, A. J., Painter, S. C., Young, J. R., Bates, N. R., Bowler, B., Drapeau, D., Lyczsckowski, E., and Balch, W. M.: The 2008 *Emiliania huxleyi* bloom along the patagonian shelf: Ecology, biogeochemistry, and cellular calcification, Global Biogeochem. Cy., 27, 2013GB004641, doi:10.1002/2013GB004641, 2013.

Putt, M.: Abundance, chlorophyll content and photosynthetic rates of ciliates in the Nordic Seas during summer, Deep-Sea Res., 37, 1713-1731, doi:10.1016/0198-0149(90)90073-5, 1990.

Ragueneau, O. and Tréguer, P.: Determination of biogenic silica in coastal waters: applicability and limits of the alkaline digestion method, Mar. Chem., 45, 43-51, doi:10.1016/0304-4203(94)90090-6, 1994.

Rees, A. P., Joint, I., and Donald, K. M.: Early spring bloom phytoplankton-nutrient dynamics at the Celtic Sea Shelf Edge, Deep-Sea Res Pt I, 46, 483-510, doi:10.1016/s0967-0637(98)00073-9, 1999.

Rynearson, T., Richardson, K., Lampitt, R., Sieracki, M., Poulton, A., Lyngsgaard, M., and Perry, M.: Major contribution of diatom resting spores to vertical flux in the sub-polar North Atlantic, Deep-Sea Res Pt I, 82, 60-71, doi:10.1016/j.dsr.2013.07.013, 2013.

Sanders, R., Henson, S. A., Koski, M., De La Rocha, C. L., Painter, S. C., Poulton, A. J., Riley, J., Salihoglu, B., Visser, A., Yool, A., Bellerby, R., and Martin, A.: The biological carbon pump in the North Atlantic, Prog. Oceanogr., 129, 200-218, doi:10.1016/j.pocean.2014.05.005, 2014.

Sanders, R., Morris, P. J., Stinchcombe, M., Seeyave, S., Venables, H., and Lucas, M.: New production and the *f* ratio around the Crozet Plateau in austral summer 2004–2005 diagnosed from seasonal changes in inorganic nutrient levels, Deep-Sea Res. Pt. II, 54, 2191-2207, doi:10.1016/j.dsr2.2007.06.007, 2007.

876 Savidge, G., Boyd, P., Pomroy, A., Harbour, D., and Joint, I.: Phytoplankton production and
877 biomass estimates in the northeast Atlantic Ocean, May–June 1990, Deep-Sea Res Pt I, 42,
878 599-617, doi:10.1016/0967-0637(95)00016-Y, 1995.

879 Siegel, D., Doney, S., and Yoder, J.: The North Atlantic spring phytoplankton bloom and
880 Sverdrup's Critical Depth Hypothesis, Science, 296, 730, doi:10.1126/science.1069174,
881 2002.

882 Sieracki, M. E., Verity, P. G., and Stoecker, D. K.: Plankton community response to
883 sequential silicate and nitrate depletion during the 1989 North Atlantic spring bloom,
884 Deep-Sea Res. Pt. II, 40, 213-225, doi:10.1016/0967-0645(93)90014-E, 1993.

885 Smetacek, V. S.: Role of sinking in diatom life-history cycles: ecological, evolutionary and
886 geological significance, Mar. Biol., 84, 239-251, doi:10.1007/BF00392493, 1985.

887 Smyth, T. J., Allen, I., Atkinson, A., Bruun, J. T., Harmer, R. A., Pingree, R. D.,
888 Widdicombe, C. E., and Somerfield, P. J.: Ocean net heat flux influences seasonal to
889 interannual patterns of plankton abundance, PLoS ONE, 9, e98709,
890 doi:10.1371/journal.pone.0098709, 2014.

891 Stoecker, D. K.: Mixotrophy among dinoflagellates, J. Eukaryot. Microbiol., 46, 397-401,
892 doi:10.1111/j.1550-7408.1999.tb04619.x, 1999.

893 Sverdrup, H.: On conditions for the vernal blooming of phytoplankton, J. Conseil Int. Explor.
894 Mer, 18, 287-295, 1953.

895 Taylor, J. R. and Ferrari, R.: Ocean fronts trigger high latitude phytoplankton blooms,
896 Geophys. Res. Lett., 38, doi:10.1029/2011GL049312, 2011a.

897 Taylor, J. R. and Ferrari, R.: Shutdown of turbulent convection as a new criterion for the
898 onset of spring phytoplankton blooms, Limnol. Oceanogr., 56, 2293,
899 doi:10.4319/lo.2011.56.6.2293, 2011b.

900 Townsend, D. W., Cammen, L. M., Holligan, P. M., Campbell, D. E., and Pettigrew, N. R.:
901 Causes and consequences of variability in the timing of spring phytoplankton blooms,
902 Deep-Sea Res Pt I, 41, 747-765, doi:10.1016/0967-0637(94)90075-2, 1994.

903 Townsend, D. W., Keller, M. D., Sieracki, M. E., and Ackleson, S. G.: Spring phytoplankton
904 blooms in the absence of vertical water column stratification, Nature, 360, 59-62,
905 doi:10.1038/360059a0, 1992.

906 Weiss, R. F.: Carbon dioxide in water and seawater: the solubility of a non-ideal gas, Mar.
907 Chem., 2, 203-215, doi:10.1016/0304-4203(74)90015-2, 1974.

908 Young, J. R., Geisen, M., Cros, L., Kleijne, A., Sprengel, C., Probert, I., and Ostergaard, J.: A
909 guide to extant coccolithophore taxonomy, J. Nannoplankt. Res. Special Issue, 1, 1-132,
910 2003.

911 Zubkov, M. V., Burkill, P. H., and Topping, J. N.: Flow cytometric enumeration of DNA-
912 stained oceanic planktonic protists, J Plankton Res, 29, 79-86, doi:10.1093/plankt/fbl059,
913 2007.

914

Table 1: Physicochemical features of the Iceland Basin and Norwegian Basin stations: SST, sea surface temperature; SSS, sea surface salinity; CT, dissolved inorganic carbon; ΩC, calcite saturation state; NO3, nitrate; PO4, phosphate; dSi, silicic acid.

						Carbonate Chemistry			Surface Macronutrients (mmol m^{-3})		
Location	Sta.	Date	Day of Year	SST (°C)	SSS	C_T (µmol m^{-3})	pH_T	Ω_C	NO_3	PO_4	dSi
Iceland Basin	1	25 Mar	85	8.7	35.3	2149	8.0	3.1	12.3	0.79	4.7
	1	26 Mar	86	8.7	35.3	2148	8.0	3.1	12.6	0.81	4.7
	2	7 Apr	98	8.7	35.3	2140	8.0	3.1	12.4	0.81	4.5
	2	10 Apr	101	8.7	35.3	2139	8.1	3.2	11.5	0.75	4.3
	3	18 Apr	109	8.8	35.3	2144	8.1	3.2	11.6	0.79	4.3
	3	19 Apr	110	8.7	35.3	2150	8.1	3.2	11.9	0.76	4.1
	4	27 Apr	118	8.9	35.3	2135	8.1	3.2	10.7	0.70	3.1
	4	29 Apr	120	8.6	35.3	2148	-	-	12.0	0.80	4.2
Norwegian Basin	1	30 Mar	90	7.0	35.2	2142	8.1	3.0	12.1	0.67	5.3
	1	31 Mar	91	7.1	35.2	2161	8.1	3.0	12.5	0.81	5.4
	2	12 Apr	103	7.2	35.2	2153	8.1	3.0	13.4	0.84	5.6
	2	14 Apr	105	6.9	35.2	2152	8.1	3.0	13.5	0.82	5.6
	3	22 Apr	113	6.5	35.1	2150	8.1	3.0	12.2	0.79	5.7
	3	25 Apr	116	6.8	35.2	2143	8.1	3.0	12.5	0.82	5.7

Table 2: Biological features of the Iceland Basin and Norwegian Basin stations: Chl *a*, chlorophyll *a*; PP, primary production; $bSiO_2$, particulate silicate; PIC, particulate inorganic carbon.

						Surface size fractions			Euphotic zone integrals			
Location	Sta.	Date	Day of Year	Surface Chl *a* (mg m^{-3})	Surface PP (mmol C m^{-3} d^{-1})	>10 µm Chl *a* (%)	>10 µm PP (%)	Euphotic zone depth (m)	Chl *a* (mg m^{-2})	$bSiO_2$ (mmol Si m^{-2})	PIC (mmol C m^{-2})	PP (mmol C m^{-2} d^{-1})
Iceland Basin	1	25 Mar	85	0.27		28		115	22.3	8.3	7.7	
	1	26 Mar	86	0.31	0.41	24	35	115	26.5	2.5	4.5	22.2
	2	7 Apr	98	1.13		80		72	61.4	8.7	8.7	
	2	10 Apr	101	2.18	4.89	84	61	72	146.4	19.6	6.9	221.9
	3	18 Apr	109	1.01		56		50	49.2	13.4	6.5	
	3	19 Apr	110	1.15	2.11	67	40	50	55.6	15.4	5.8	58.0
	4	27 Apr	118	1.18		-		86	75.7	37.1	11.0	
	4	29 Apr	120	0.62	1.19	94	61	86	55.3	27.6	8.1	61.5
Norwegian Basin	1	30 Mar	90	0.58		6		80	34.6	5.5	7.7	
	1	31 Mar	91	0.59	0.67	7	5	80	39.2	7.0	7.1	27.3
	2	12 Apr	103	0.54		9		65	32.3	4.4	5.9	
	2	14 Apr	105	0.69	0.90	13	5	65	37.2	4.4	6.4	38.2
	3	22 Apr	113	0.93		10		56	46.7	5.0	9.7	
	3	25 Apr	116	0.84	1.11	21	20	56	40.5	6.4	10.5	39.8

Table 3: Surface phytoplankton abundance at the Iceland Basin and Norwegian Basin stations, measured by flow cytometry (*Synechococcus*, pico-eukaryotes and nanoplankton), inverted microscopy (diatoms and microzooplankton) and polarizing light microscopy (coccolithophores).

					Phytoplankton abundance (cells mL^{-1})								
										Coccolithophores			
Location	Sta.	Date	Day of Year	Depth (m)	*Synechococcus*	Pico-eukaryotes	Nanoplankton (<10 µm)	Diatoms (>10 µm)	Micro-zooplankton	*E. huxleyi*	*C. pelagicus*	*A. robusta*	Others
Iceland Basin	1	25 Mar	85	5	-	-	-	-	-	7.5	0.15		1.2
	1	26 Mar	86	15	675	2347	1116	1.3	2.5	4.4	0.22		0.5
	2	7 Apr	98	5	400	3375	215	-	-	5.2	0.19		4.1
	2	10 Apr	101	10	480	6715	813	249.2	4.0	6.8	0.15		0.7
	3	18 Apr	109	5	-	-	-	-	-	16.9	0.22		25.6
	3	19 Apr	110	7	2112	6962	712	151.3	2.8	21.9	0.69		22.3
	4	27 Apr	118	8	1299	1486	298	-	-	26.7	0.81		7.9
	4	29 Apr	120	11	782	1215	313	87.8	4.7	13.2	0.84		7.5
Norwegian Basin	1	30 Mar	90	8	-	-	-	-	-	6.1	0.09	4.8	2.9
	1	31 Mar	91	10	2617	18016	484	0.2	10.8	7.2	0.28	3.8	1.0
	2	12 Apr	103	8	-	-	-	-	-	11.8	0.41	2.7	0.3
	2	14 Apr	105	10	3372	10433	858	0.1	17.6	16.0	0.38	3.7	5.1
	3	22 Apr	113	7	-	-	-	-	-	27.9	2.66	12.7	11.7
	3	25 Apr	116	7	5483	8456	1384	0.5	14.0	28.1	2.79	7.8	8.6

Figure Captions

Fig. 1: Sampling locations in the Iceland Basin (ICB) and the Norwegian Basin (NWB), superimposed on a composite of MODIS sea surface temperature for 25 March – 29 April 2012.

Fig. 2: Upper water column profiles for the ICB (A, B, C) and the NWB (D, E, F), of A,D) density, B,E) CTD fluorescence and C,F) CTD fluorescence normalised to peak CTD fluorescence for each profile.

Fig. 3: Seasonal variation in A) satellite sea surface temperature (SST), B) satellite daily incidental PAR and day length and C,D) satellite chlorophyll *a* (Chl *a*) for C) the Iceland Basin (ICB) and D) the Norwegian Basin (NWB) for 2012. The grey region indicates the period of the cruise. The vertical dotted lines in plots C and D indicate bloom initiation, calculated following Henson et al. (2009). The insets in C & D show the variation in satellite chlorophyll during the period of the cruise.

Fig. 4: Surface (5-15 m) measurements of A) Particulate silicate ($bSiO_2$) and B) diatom species abundance in the Iceland Basin. Black symbols indicate where diatoms were counted from Lugol's samples, while open symbols indicate SEM counts.

Fig. 5: Size fractionated chlorophyll *a* (Chl *a*) for A, C) the Iceland Basin, and B, D) the Norwegian Basin. Plots A and B show the < 10 µm and > 10 µm fractions, C and D show the < 2µm, 2-10 µm, 10-20 µm, and > 20 µm fractions.

Fig. 1

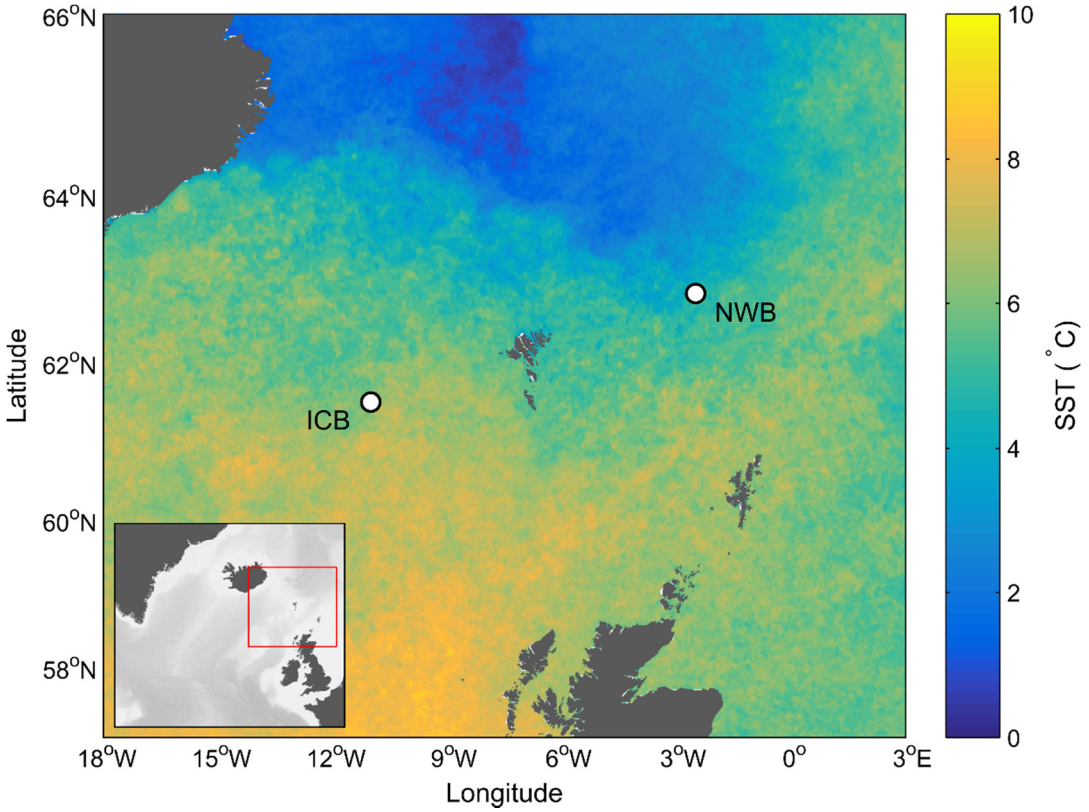
66°N
64°N
62°N
60°N
58°N
Latitude
18°W
15°W
12°W
9°W
6°W
3°W
0°
3°E
Longitude
NWB
ICB
10
8
6
4
2
0
SST (°C)

36 **Fig. 2**

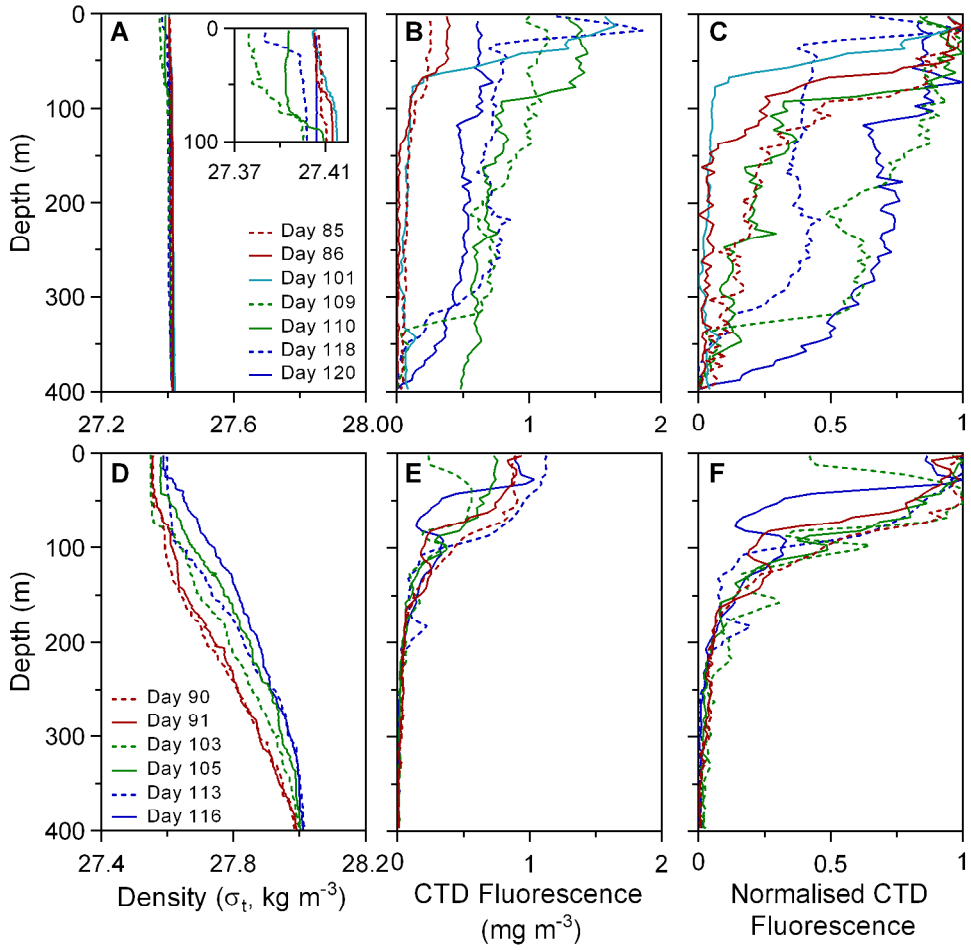
A
B
C
D
E
F
Depth (m)
0
100
200
300
400
27.2
27.6
28.00
1
2
0.5
27.37
27.41
Day 85
Day 86
Day 101
Day 109
Day 110
Day 118
Day 120
Day 90
Day 91
Day 103
Day 105
Day 113
Day 116
27.4
27.8
28.20
Density (σ_t, kg m^{-3})
CTD Fluorescence
(mg m^{-3})
Normalised CTD
Fluorescence

37

38 **Fig. 3**

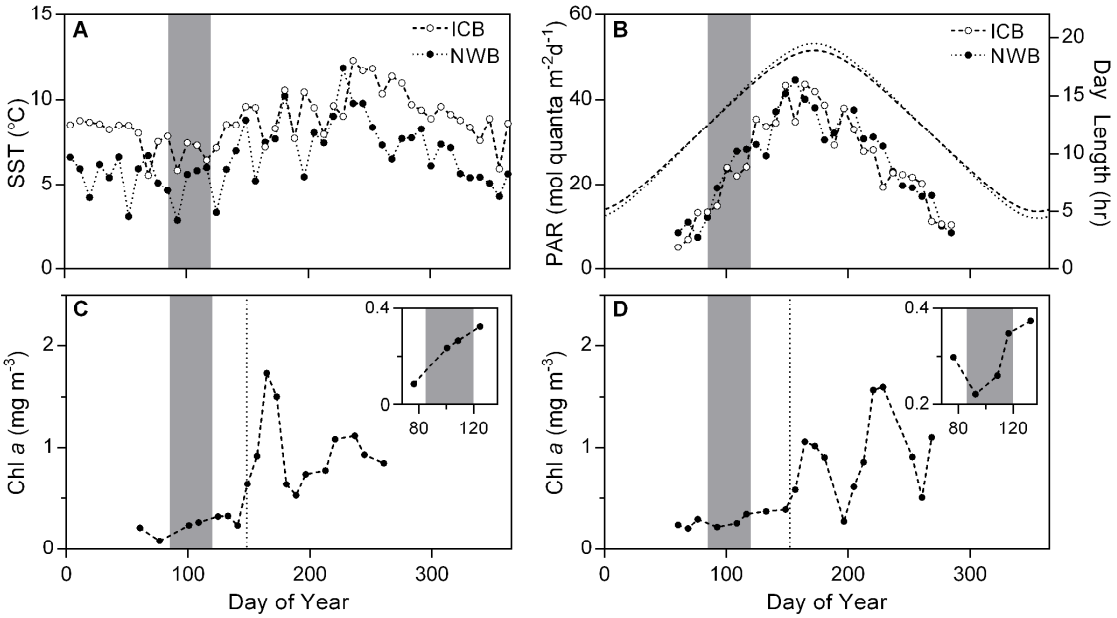
A
ICB
NWB
SST (°C)
B
PAR (mol quanta m-2d-1)
Day Length (hr)
C
Chl a (mg m-3)
D
Chl a (mg m-3)
Day of Year
Day of Year

39

40 **Fig. 4**

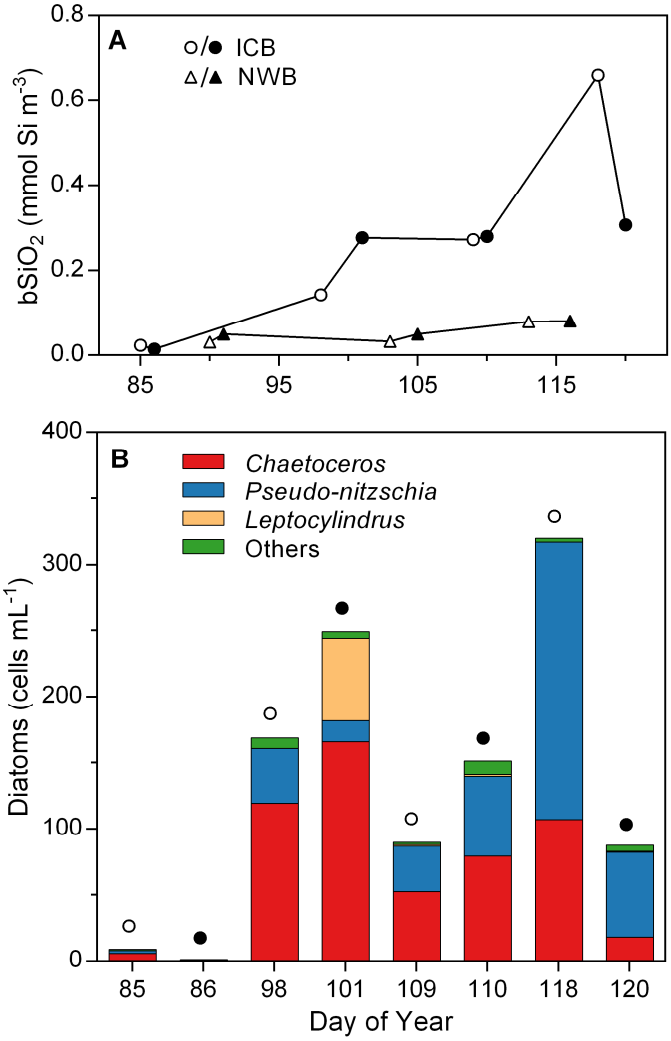
A
○/● ICB
△/▲ NWB
bSiO2 (mmol Si m-3)
0.0
0.2
0.4
0.6
0.8
85
95
105
115
B
Chaetoceros
Pseudo-nitzschia
Leptocylindrus
Others
Diatoms (cells mL-1)
0
100
200
300
400
85
86
98
101
109
110
118
120
Day of Year

41

42

43 **Fig. 5**

44

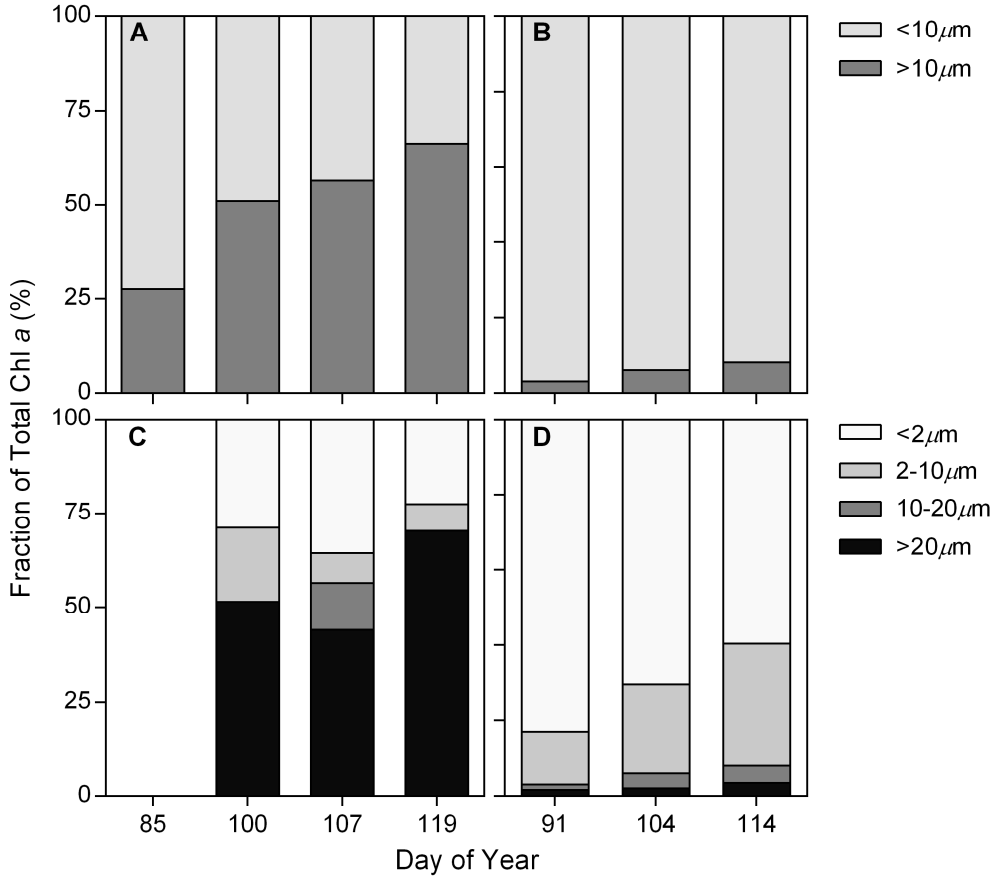
A
B
C
D
100
75
50
25
0
Fraction of Total Chl a (%)
<10μm
>10μm
<2μm
2-10μm
10-20μm
>20μm
85
100
107
119
91
104
114
Day of Year

45